IEEE Access
Multidisciplinary | Rapid Review | Open Access Journal

Received May 28, 2019, accepted July 1, 2019, date of publication July 12, 2019, date of current version August 1, 2019.

Digital Object Identifier 10.1109/ACCESS.2019.2928373

One-Dimensional Heat Conduction Inverse Modelling of Heat Flux Generated at Tool-Chip Interface in Cutting Inconel 718

JINFU ZHAO AND ZHANQIANG LIU

School of Mechanical Engineering, Shandong University, Jinan 250061, China
Key National Demonstration Center for Experimental Mechanical Engineering Education, Key Laboratory of High Efficiency and Clean Mechanical Manufacture of MQE, Jinan 250061, China

Corresponding author: Zhanqiang Liu (melius@sdu.edu.cn)

This work was supported in part by the National Science Foundation of China under Grant 51425503 and Grant 91860207, in part by the grants from Taishan Scholar Foundation, and in part by the National Key Research and Development Program of China under Grant 2018YFB2002201.

ABSTRACT Inconel 718 has been taken as the difficult-to-machine material for manufacturing aerial turbine disk due to its superior high-temperature resistance and high hardness. Massive heat flux generated at the tool-chip interface, and high tool temperature can induce severe tool wear in cutting Inconel 718 with cemented carbide tool. Determining the generated heat flux and tool temperature in the cutting process is crucial to illustrate the tool wear mechanism. However, there is a shortage of method for integrated estimation of the heat flux generated at the tool-chip interface and temperature distribution within the tool in cutting Inconel 718. In the current study, the one-dimensional inverse heat conduction model was proposed for the integrated prediction of generated heat flux and tool temperature. First, the heat flux generated at the tool-chip interface was inversely calculated with the measured rake face temperature. The heat flux generated at tool-chip interface and heat flux dissipated into tool were increased with cutting speed. Then, the temperature distribution within the cemented carbide tool was determined with the derived analytical solution. Temperature interval between rake face temperature and reverse surface temperature was increased with cutting speed. Finally, the predicted heat flux values were verified accurate with the relative error of less than 3% compared with the research results from the modified Merchant's chip formation model. The proposed model can be used for predicting heat flux and temperature distribution for other tool and workpiece pairs.

INDEX TERMS One-dimensional inverse heat conduction model, cemented carbide tool, temperature distribution within tool, Inconel 718, heat flux generated at tool-chip interface.

I. INTRODUCTION

Inconel 718 is commonly applied for manufacturing aerial turbine disk due to its superior high-temperature resistance, high thrust-weight ratio and good corrosion resistance [1]. For the low thermal conductivity and high hardness of Inconel 718, massive heat flux is induced at the interface between the moving chip of Inconel 718 and rake face of cemented carbide tool [2], [3]. The massive generated heat flux, and high tool temperature can cause severe tool wear to decrease tool life [4], [5]. Determining the generated heat flux and tool temperature is crucial to illustrate tool wear mechanism [6], [7].

The associate editor coordinating the review of this manuscript and approving it for publication was Rajeeb Dey.

The generated heat flux can be predicted from two ways. The first way is to predict the generated heat flux by calculating the friction work at the interface between moving chip and tool rake face, which can be calculated with the modified Merchant's chip formation model [8]. The solution process of modified Merchant's chip formation model is depicted in the Appendix. Ghani *et al.* [9] utilized the modified Merchant's chip formation model to calculate the heat flux generated at tool-chip interface in cutting process of H13 steel with CBN tool. They confirmed that this model can well predict the heat flux generated in dry cutting process.

The other way is to predict the generated heat flux by measuring surface heat conduction rate, which is derived from the variation of surface temperature with time. Mzard *et al.* [10], [11] calculated the generated heat flux

with the measured surface temperature variation. The surface temperature variation with time was measured with infrared thermometer. The generated heat flux was determined by the step change of surface temperature variation with the one-dimensional semi-infinite medium solution and Duhamel' superposition integral. Samadi *et al.* [12] calculated the heat flux dissipated into tool body in finite element (FE) model with the sequential function specification method. The dissipated heat flux was estimated with inverse algorithm. The calculated results showed that the temperature-dependent thermo-physical properties of material should be considered to determine the generated heat flux. Huang and Lo [13] predicted the heat flux distribution in cutting tools with FE model established by Ansys CFX 4.4. The predicted heat fluxes were determined with the inverse algorithm of steepest descent method. The temperature-dependent thermo-physical properties of material were considered to obtain better prediction accuracy.

Some researchers have predicted the temperature distribution within tool body. Komanduri and Hou [14] determined the generated heat flux with the modified Merchant's chip formation model. The temperature distribution within tool body was obtained with the moving heat source method through complex solutions. Shan*et al.* [15] proposed a modified model for determining tool temperature in machining Ti6Al4V based on Komanduri-Hou model and Huang-Liang model [16]. The tool temperature was determined with the moving heat source method considering the tool-chip heat partition coefficient. The model was verified accurate with the interval temperature measured with the embedded thermocouple in dry orthogonal cutting experiment. Zhao *et al.* [17] predicted temperature distribution within cemented carbide tool with one-dimensional heat transfer model by applying constant temperature on tool rake face. The proposed method was verified convenient and valid with the simulating experiment.

However, the surface temperature variation is hard to be accurately recorded with duration time. Thus, the generated heat flux is with difficulty to be inversely calculated with the surface heat transfer rate [10]–[13]. The temperature distribution within tool body is difficult to be obtained due to the complex calculation of moving heat source method [14]–[16]. The generated heat flux cannot be determined with the heat transfer model proposed by Zhao and Liu [17] due to the assumed constant rake face temperature. There is a shortage of method for integrated estimation of the generated heat flux and tool temperature in cutting Inconel 718.

In this research, we aim to propose a model for integrated estimation of the heat flux generated at tool-chip interface and tool temperature in cutting Inconel 718. Firstly, the one-dimensional inverse heat conduction model of cemented carbide tool was established. Then, the generated heat flux was inversely calculated with the cutting temperature measured by two-color thermometer [18]. Lastly, the temperature distribution within cemented carbide tool was determined. The predicted heat flux values were verified accurate with the former research results from the modified Merchant's chip formation model.

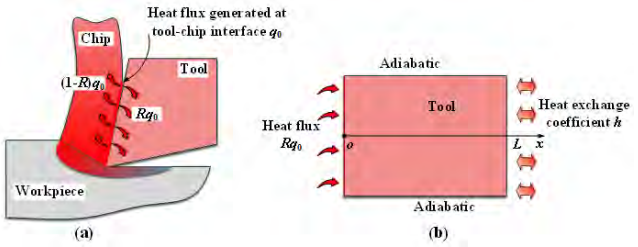

FIGURE 1. (a) Heat partition schematic at tool-chip interface in cutting Inconel 718 with cemented carbide tool; (b) One-dimensional heat conduction model of cemented carbide tool.

II. MODEL AND SOLUTIONS OF HEAT FLUX GENERATED AT TOOL-CHIP INTERFACE AND TEMPERATURE DISTRIBUTION WITHIN TOOL BODY IN CUTTING INCONEL 718

As depicted in Fig. 1, the heat flux generated at tool-chip interface is defined as q_0. The heat partition coefficient R_T is defined as the percentage of generated heat flux dissipated into tool body. As illustrated by Grzesik *et al.* [19], [20], the heat partition coefficient R_T can be defined with Eq. (1).

$$R_T = \frac{3\lambda_T\sqrt{\alpha_W}}{2\lambda_W\sqrt{\alpha_T} + 3\lambda_T\sqrt{\alpha_W}} \tag{1}$$

where λ_T and λ_W are the thermal conductivity of cemented carbide tool and workpiece, respectively. α_T and α_W are the thermal diffusivity of cemented carbide tool and workpiece, respectively.

The heat flux dissipated into tool body is assumed as $R_T q_0$. The heat flux dissipated into the moving chip is assumed as $(1 - R_T)q_0$. The one-dimensional heat conduction model is established from the radium point in tool-chip contact area with the x-coordinate perpendicular to the rake face of cemented carbide tool. As illustrated in researches [17], the heat exchange coefficient h at tool-cutter arbor interface can be assumed as constant 4971 W/(m$^{2\cdot}$°C). The heat convection between the tool and environment air (temperature $T_\infty = 25$ °C) can be neglected compared with the severe heat conduction within tools. The upper and bottom surface of the established model are assumed as adiabatic.

A. ANALYTICAL SOLUTION OF TEMPERATURE DISTRIBUTION WITHIN CEMENTED CARBIDE TOOL IN CUTTING INCONEL 718

Partial derivative equation for the thermal model in Fig. 1(b) can be illustrated with Eq. (2).

$$\frac{\partial^2 T}{\partial x^2} = 0, \quad 0 \le x \le L \tag{2}$$

Outer boundary conditions for the thermal model in Fig. 1(b) are expressed with Eqs. (3) and (4).

$$\lambda_T \frac{\partial T}{\partial x}|_{x=0} = \lambda_T \frac{\partial T}{\partial x}|_{x=L} = R_T q_0 \tag{3}$$

$$\lambda_T \frac{\partial T}{\partial x}|_{x=L} = h(T|_{x=L} - T_\infty) \tag{4}$$

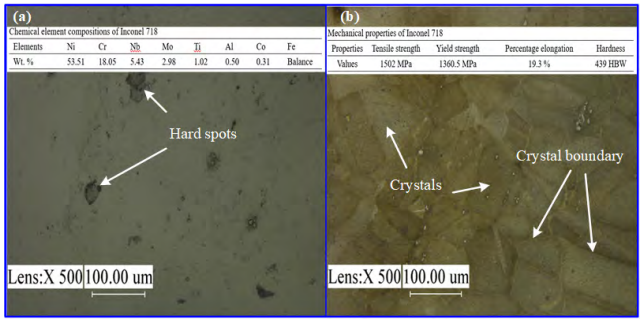

FIGURE 2. Optical microscope image of Inconel 718 (a) Polished surface; (b) Corroded surface.

The analytical solution of temperature distribution within cemented carbide tool in cutting Inconel 718 was derived with Eq. (5).

$$T(x) = -\frac{R_T q_0}{\lambda_T} x + \frac{R_T q_0}{\lambda_T} L + \frac{R_T q_0}{h} + T_\infty, \quad 0 < x < L \tag{5}$$

B. ANALYTICAL SOLUTION OF HEAT FLUX GENERATED AT TOOL-CHIP INTERFACE IN CUTTING iNCONEL 718 WITH CEMENTED CARBIDE TOOL

The generated heat flux can be predicted with two analytical methods. The first analytical method is to inversely compute the generated heat flux with Eq. (5) by measuring tool rake face temperature. The analytical solution of generated heat flux is inversely defined with Eq. (6).

$$q_0 = \frac{(T_{x=0} - T_\infty)\,\lambda_T h}{R_T\,(\lambda_T + hL)} \tag{6}$$

The second analytical method is to inversely compute the generated heat flux with Eq. (5). The temperature of the internal embedded point for K-type thermocouple within tool body is measured. The analytical solution of generated heat flux is inversely defined with Eq. (7).

$$q_0 = \frac{(T(x) - T_\infty)\,\lambda_T h}{R_T\,(\lambda_T - hx + hL)}, \quad 0 < x < L \tag{7}$$

III. MATERIAL AND EXPERIMENT DESIGN

A. MATERIAL CHARACTERIZATION

As depicted in Fig. 2, the optical microscope image for the workpiece of Inconel 718 was obtained with the large depth of field three-dimensional micro-system VHX-600E. The corroded surface of Inconel 718 was obtained by aqua regia within the duration time about 15 s. The phase composition and metallographic structure for the cemented carbide tool of Kennametal carbide 2210 were summarized in former research [21]. The thermal properties of Inconel 718 and substrate carbide were summarized in Figs. 3-5, respectively.

B. EXPERIMENT DESIGN

As depicted in Fig. 6, dry turning experiment was conducted in CNC turning center. The cemented carbide tool

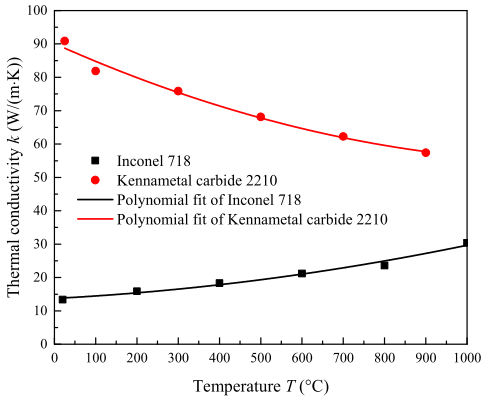

FIGURE 3. Temperature-dependent thermal conductivity of Inconel 718 and Kennametal carbide 2210.

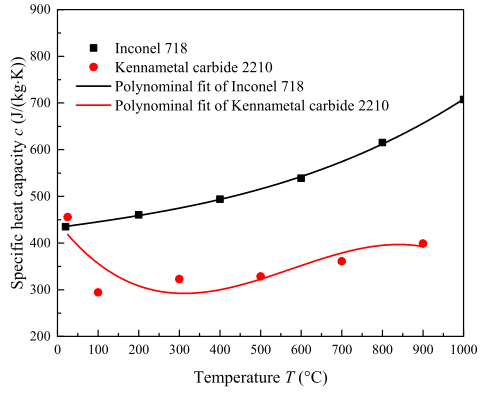

FIGURE 4. Temperature-dependent specific heat capacity of Inconel 718 and Kennametal carbide 2210.

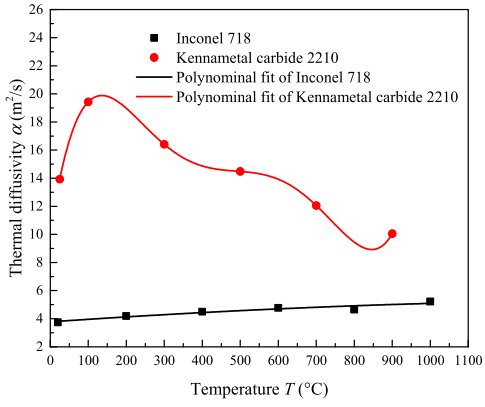

FIGURE 5. Temperature-dependent thermal diffusivity of Inconel 718 and Kennametal carbide 2210.

was obtained from Kennametal company with the type of "CNMG120408MS K313". The thickness of tool body was measured as 4.5 mm. The cemented carbide tool was with rake face angle γ 15°, cutting edge angle κ 5°, clearance angle α 6° and nose radius r_ε 0.8 mm.

The workpiece of Inconel 718 was machined as a cylinder with the length 30 mm and diameter ϕ130 mm. The cutting speed v_c was assumed as 30, 60, 90, 120 m/min, respectively.

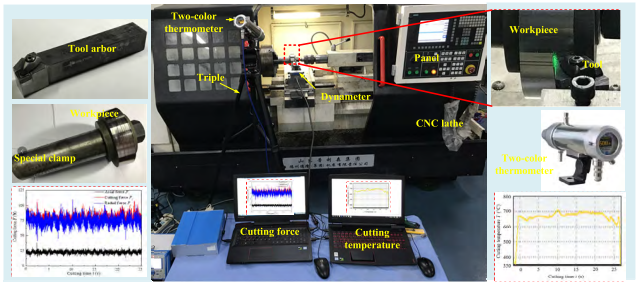

FIGURE 6. (a) Experimental setup of dry turning Inconel 718; (b) Cutting temperature variation with time at cutting speed 90 m/min; (c) Measured force variation with time at cutting speed 90 m/min.

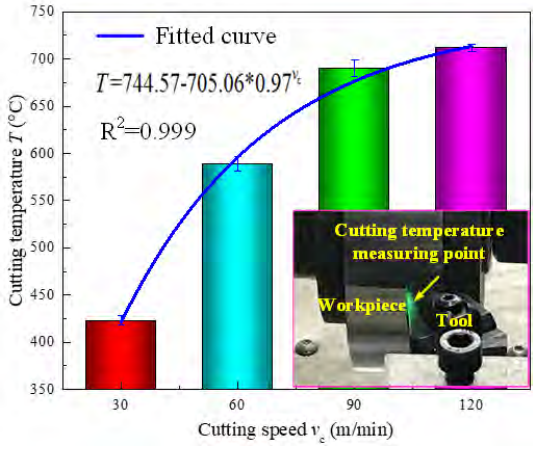

FIGURE 7. Measured cutting temperature within cutting speed ranges 30-120 m/min.

The feed f was assumed as 0.1 mm/rev and cutting depth a_p was assumed as 0.1 mm.

Cutting temperature in turning Inconel 718 was measured with the two-color thermometer. The measuring principle of two-color thermometer has been illustrated in former research [18]. One is noted that the cutting temperature was externally observed and measured in the chip which just flowed from cutting zone. The just flowed chip temperature was equal to the tool rake face temperature $T_x = 0$ as mentioned in Eq. (6).

The cutting forces were needed to be obtained to calculate the generated heat flux with the modified Merchant's chip formation model. The cutting forces in dry turning Inconel 718 with cemented carbide tool were measured with Kistler 9257B multicomponent dynamometer.

IV. RESULTS AND DISCUSSION

A. HEAT FLUX GENERATED AT TOOL-CHIP INTERFACE

Cutting temperature measured with the two-color thermometer was depicted in Fig. 7. The fitted curve was obtained with the form of exponential function. The increasing rate of measured cutting temperature with cutting speed was gradually decreased with cutting speed.

The material was assumed at the constant temperature under each cutting speed as depicted in Fig. 7. According to

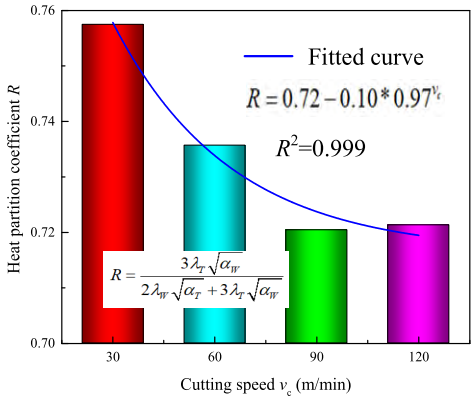

FIGURE 8. Calculated heat partition coefficient within cutting speed ranges 30-120 m/min.

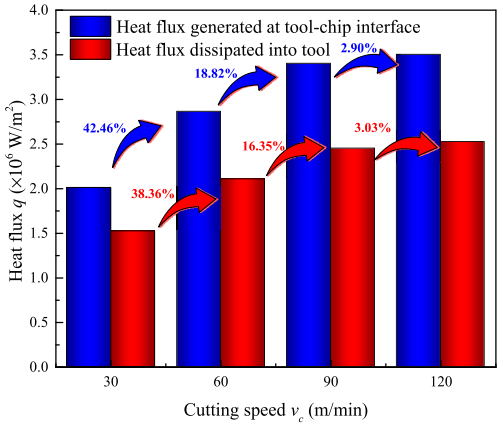

FIGURE 9. Variation of the heat flux generated at tool-chip interface and the heat flux dissipated into tool body with cutting speed in the cutting process of Inconel 718 with cemented carbide tool.

Figs. 3-5, the thermal properties of Inconel 718 and cemented carbide tool were determined as the value at corresponding temperature with the scale difference method. Under each cutting speed, the heat partition coefficient was calculated with the specific thermal property of Inconel 718 and Kennametal carbide 2210 according to Eq. (1).

The calculated heat partition coefficient was plotted in Fig. 8. The heat partition coefficient was decreased with increasing cutting speed in the form of exponential function. As referred to Figs. 3 and 5, the tool thermal conductivity and tool thermal diffusivity were decreased with increasing temperature. The decrease of tool thermal conductivity and tool thermal diffusivity can prevent more heat flux dissipate into tool body, thus inducing lower heat partition coefficient.

The heat flux q_0 generated at tool-chip interface was calculated with Eq. (6). The heat flux dissipated into tool body was calculated as $R_T q_0$. The variations of generated heat flux and heat flux dissipated into tool with cutting speed in the cutting process of Inconel 718 with cemented carbide tool were listed in Fig. 9.

The heat flux q_0 and $R_T q_0$ were increased with cutting speed. The increment of generated heat flux q_0

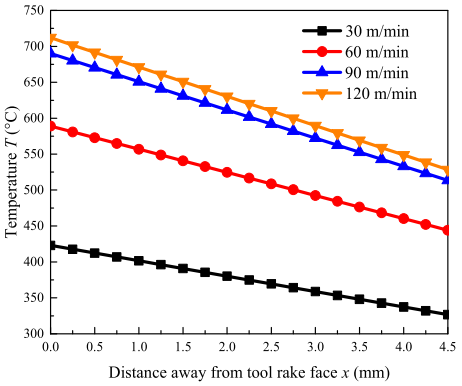

FIGURE 10. Temperature distribution within cemented carbide tool body away from rake face within cutting speed ranges 30-120 m/min.

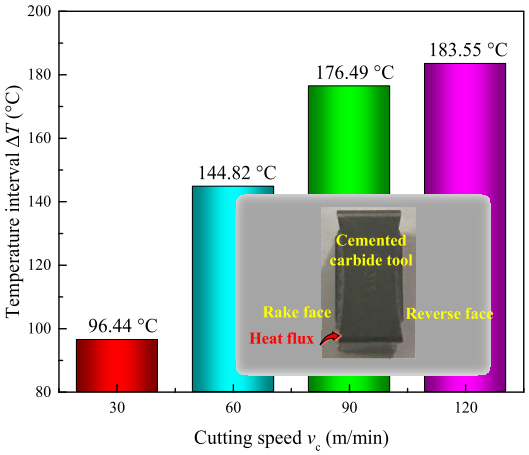

FIGURE 11. Temperature interval between tool rake face temperature and tool reverse face temperature within cutting speed ranges 30-120 m/min.

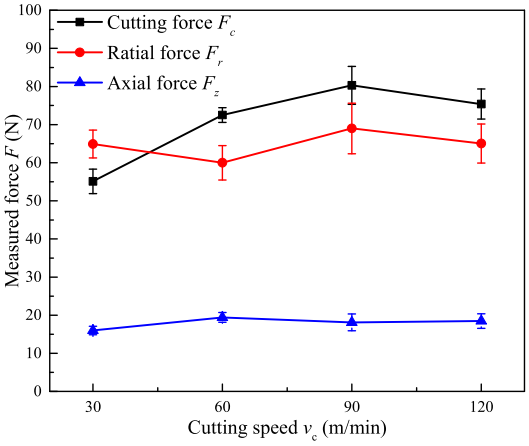

FIGURE 12. Variations of measured cutting force F_c, radial force F_r and axial force F_z with cutting speed in dry turning Inconel 718 with cemented carbide tool.

was 0.8543×10^6, 1.3936×10^6, 1.4924×10^6 W/m^2 for 60, 90, 120 m/min compared with the generated heat flux 2.0118×10^6 W/m^2 at cutting speed 30 m/min, respectively. The increment rate of generated heat flux was 42.46%, 69.27%, 74.18% for 60, 90, 120 m/min compared with the generated heat flux at cutting speed 30 m/min, respectively.

The increment of heat flux Rq_0 dissipated into tool body was 0.5846×10^6, 0.9293×10^6, 1.0035×10^6 W/m^2 for 60, 90, 120 m/min compared with the dissipated heat flux 1.5240×10^6 W/m^2 at cutting speed 30 m/min, respectively. The increment rate of heat flux dissipated into tool was 38.36%, 60.98%, 65.85% for 60, 90, 120 m/min compared with the heat flux dissipated into tool body at cutting speed 30 m/min, respectively. The increment rate of heat flux dissipated into tool body with cutting speed was lower than the increment rate of generated heat flux with cutting speed. It may be illustrated that the heat partition coefficient was decreased with increasing cutting speed, and the decreasing rate was increased with cutting speed. Thus, more generated heat flux can be prevented dissipate into tool body with increasing cutting speed.

B. TEMPERATURE DISTRIBUTION WITHIN CEMENTED CARBIDE TOOL BODY

The temperature distribution within tool body can be calculated with Eq. (5) as depicted in Fig. 10. The temperature was decreased with the increase of distance away from rake face. Temperature interval ΔT was proposed to analyze the temperature decrease between the rake face temperature and the reverse surface temperature of cemented carbide tool. The temperature interval ΔT within cutting speed ranges of 30-120 m/min was depicted in Fig. 11.

The temperature interval between rake face temperature and reverse face temperature of cemented carbide tool was increased with cutting speed. The increment of temperature interval was 48.38, 80.05, 87.11 °C for 60, 90, 120 m/min compared with the temperature interval 96.44 °C at cutting speed 30 m/min, respectively. The increment rate of temperature interval was 50.17%, 83.00%, 90.33% for 60, 90, 120 m/min compared with the temperature interval at cutting speed 30 m/min, respectively. The increase of temperature interval within tool body may induce severer tool thermal damage under higher cutting speed.

C. VERIFICATION

In order to verify the proposed model, the former modified Merchant's chip formation model was utilized to calculate the heat flux generated at tool-chip interface. The variations of measured cutting force F_c, radial force F_r and axial force F_z with cutting speed were depicted in Fig. 12. The generated heat flux at tool-chip interface can be calculated with Eqs. (8a)-(12a) in the Appendix.

The comparisons between the generated heat flux determined with the one-dimensional inverse heat conduction model and modified Merchant's chip formation model were depicted in Fig. 13. In order to obtain the accuracy of proposed model, the relative error for the inverse model was obtained compared with Merchant's model. The variation of relative error with cutting speed was plotted in Fig. 14. The relative error was less than 3% within cutting speed ranges 30-120 m/min.

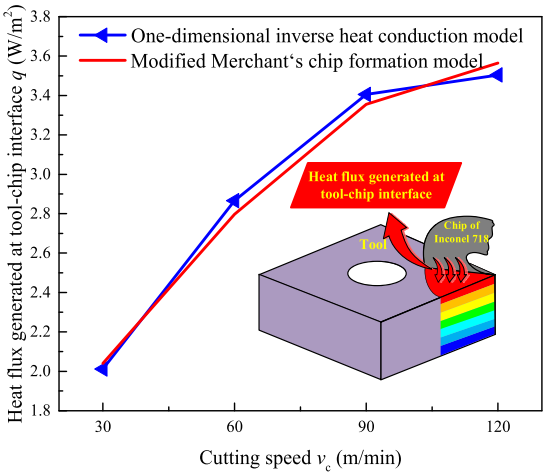

FIGURE 13. Comparisons between the generated heat flux determined with one-dimensional inverse heat conduction model and modified Merchant's chip formation model.

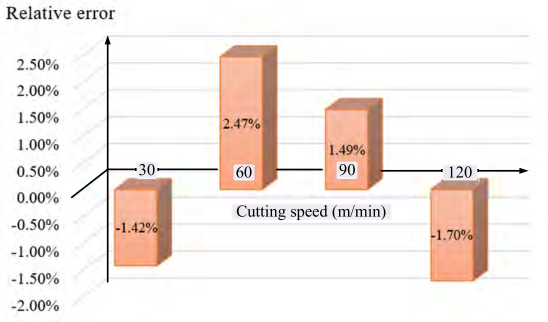

FIGURE 14. Relative error of generated heat flux determined with one-dimensional inverse heat conduction model and modified Merchant's chip formation model.

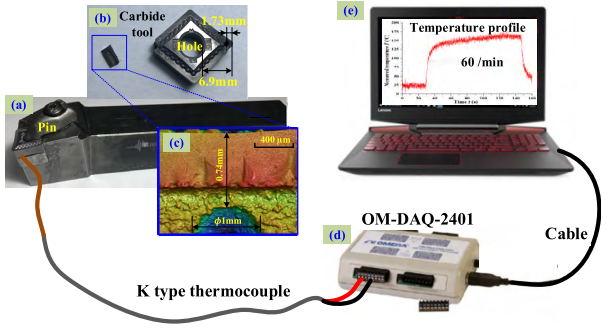

FIGURE 15. Schematic of verified experiment setup for cutting speed 60 m/min.

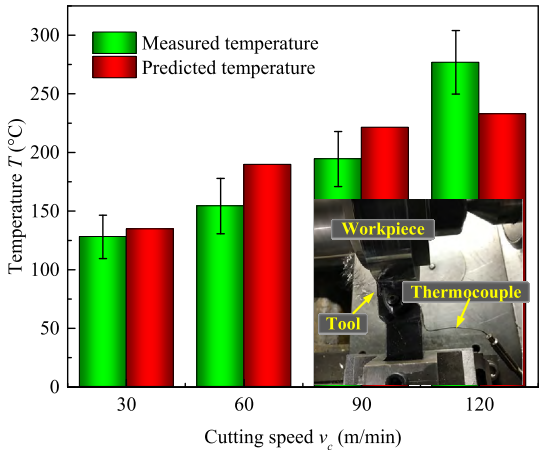

FIGURE 16. Comparisons between measured tool temperature and predicted tool temperature within cutting speed ranges 30-120 m/min.

There are some advantages of the proposed model compared with the modified Merchant's chip formation model. The cutting force, tangential force and radial force were needed to be measured for the prediction of heat flux generated at tool-chip interface with Merchant's chip formation model. There was not necessary to measure cutting forces for predicting heat flux with the proposed model. The time assumed in calculating heat flux generated at tool-chip interface with Merchant's chip formation model was about 2ms. But the calculated time by using the proposed model was only 0.5ms. The proposed model can decrease the calculated time about 75% compared with using Merchant's chip formation model (Matlab 2016a, Intel(R) Core(TM) i7-8550U CPU@1.80GHz). The temperature distribution within cemented carbide tool cannot be predicted directly with using Merchant's chip formation model. The proposed model can well predict the temperature distribution within tool body.

The schematic of verified experiment at cutting speed 60 m/min was illustrated in Fig. 15. As shown in Fig. 15(a), the temperature of internal point within carbide tool was measured with the embedded K-type thermocouple (WRNK-191, diameter ϕ0.5 mm, length 3000mm). As shown in Fig. 15(b), the embedded hole was made with the electrical discharge machining (EDM), the distance of which away from the cutting zone was about 1.73 mm. As shown in Fig. 15(c), the diameter of embedded hole was about ϕ1 mm. The distance of the embedded point away from tool rake face was about 0.74 mm. The distance of the embedded point away from cutting zone can be calculated as 1.88 mm according to the Pythagorean theorem at cutting speed 60 m/min. By analogy, the distance of the embedded point away from cutting zone can be calculated as 1.90 mm, 1.98 mm, and 1.89 mm at cutting speeds 30 m/min, 90 m/min and 120 m/min, respectively. One is noted that the tool thickness should be modified as 6.9 mm as shown in Fig. 15(b) with consideration of heat transfer direction. The heat exchanging coefficient between the tool hole and fixed pin was defined as 10^6 W/(m^2· K). Thus, the temperature of embedded point can be predicted with Eq. (5).

As shown in Fig. 15(d), the electric signals generated by thermocouple were collected with the multiple channel USB data acquisition module OM-DAQ-2401 (response time 2 ms). The temperature profile with time was depicted in the personal computer with the help of specific software as shown in Fig. 15(e).

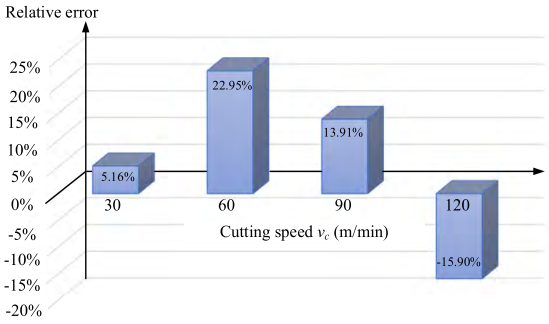

FIGURE 17. Relative error of temperature at embedded point between the predicted model and the experimental measurement within cutting speed ranges 30-120 m/min.

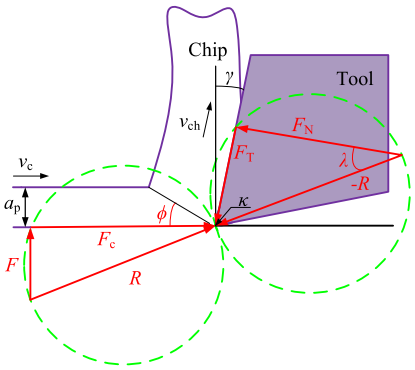

FIGURE 18. Schematic of modified Merchant's chip formation model.

The comparison between the measured temperature and predicted temperature was depicted in Fig. 16. The relative error between the predicted model and experiment was depicted in Fig. 17. The comparison results showed that the relative error between the predicted model and experimental measurement was less than 23% within cutting speed ranges 30-120 m/min. The proposed model can well predict the tool temperature in turning process.

V. CONCLUSION

In current study, one-dimensional inverse heat conduction model of cemented carbide tool is established and verified. Several conclusions are summarized as the followings.

(1) The heat flux generated at tool-chip interface and heat flux dissipated into tool were increased with cutting speed. The increment rate of generated heat flux was 42.46%, 69.27%, 74.18% for 60, 90, 120 m/min compared with the generated heat flux at cutting speed 30 m/min, respectively. The increment rate of dissipated heat flux was 38.36%, 60.98%, 65.85% for 60, 90, 120 m/min compared with the heat flux dissipated into tool body at speed 30 m/min, respectively.

(2) The temperature was decreased with the increase of distance away from rake face. Temperature interval between rake face temperature and reverse surface temperature was increased with cutting speed for cemented carbide tool. The increment rate of temperature interval was 50.17%, 83.00%, 90.33% for 60, 90, 120 m/min compared with the temperature interval at speed 30 m/min, respectively.

(3) The proposed model was verified accurate for predicting heat flux generated at tool-chip interface with the relative error less than 3% compared with the research results from modified Merchant's chip formation model within cutting speed ranges 30-120 m/min.

(4) The proposed model is verified accurate for predicting tool temperature distribution with the relative error less than 23% compared with the temperature value measured with the embedded thermocouple in turning experiment.

This study provides a useful model for integrated estimation of the generated heat flux and tool temperature distribution in cutting Inconel 718 with cemented carbide tool. The proposed model can be used for the prediction of heat flux and temperature distribution for other tool and workpiece pairs.

APPENDIX

The schematic of modified Merchant's chip formation model is depicted in Fig. 18. Where ϕ is shear angle, γ is rake face angle, κ is cut edge radius. a_p is uncut chip thickness, v_c is cutting speed and v_{ch} is chip sliding velocity. Where R and $-R$ are the two equal and opposite forces which hold the chip in equilibrium. The force R is divided into cutting force F_c and resultant feed force F. The resultant feed force F can be defined with Eq. (8a). The force $-R$ is divided into friction force F_T and normal force F_N. λ is the friction angle between normal force F_N and force $-R$.

The heat flux generated at tool-chip interface can be determined with Eqs. (8a)-(12a).

$$F = \sqrt{F_r^2 + F_z^2} \tag{8a}$$

where F_r is the radial force, F_z is the axial force.

$$\lambda = \arctan\left(\frac{F_c \sin\gamma + F\cos\gamma}{F\cos\gamma - F_f \sin\gamma}\right) \tag{9a}$$

$$F_T = F_c \sin\gamma + F\cos\gamma \tag{10a}$$

$$\phi = \frac{\pi}{4} + \gamma - \lambda \tag{11a}$$

$$w = \frac{a_p}{\sin\kappa} \tag{12a}$$

where w is the cut width.

$$v_{ch} = \frac{v_c}{\cos(\phi - \gamma)} \sin\phi \tag{10a}$$

The tool-chip contact length l_c can be defined with Eq. (11a).

$$l_c = a_p \frac{\sqrt{2}}{2\sin\phi \sin\left(\frac{\pi}{4} + \phi - \gamma\right)} \tag{11a}$$

The heat flux q_0 generated at tool-chip interface can be calculated with Eq. (12a).

$$q_0 = \frac{F_T \cdot v_{ch}}{w \cdot l_c} \tag{12a}$$

REFERENCES

[1] E. O. Ezugwu, J. Bonney, and Y. Yamane, "An overview of the machinability of aeroengine alloys," *J. Mater. Process. Technol.*, vol. 134, no. 2, pp. 233–253, 2003.

[2] D. Dudzinski, A. Devillez, A. Moufki, D. Larrouquère, V. Zerrouki, and J. Vigneau, "A review of developments towards dry and high speed machining of Inconel 718 alloy," *Int. J. Mach. Tools Manuf.*, vol. 44, no. 4, pp. 439–456, 2004.

[3] E. O. Ezugwu, "Key improvements in the machining of difficult-to-cut aerospace superalloys," *Int. J. Mach. Tools Manuf.*, vol. 45, nos. 12–13, pp. 1353–1367, 2005.

[4] D. Zhu, X. Zhang, and H. Ding, "Tool wear characteristics in machining of nickel-based superalloys," *Int. J. Mach. Tools Manuf.*, vol. 64, pp. 60–77, Jan. 2013.

[5] A. Bhatt, H. Attia, R. Vargas, and V. Thomson, "Wear mechanisms of WC coated and uncoated tools in finish turning of Inconel 718," *Tribol. Int.*, vol. 43, nos. 5–6, pp. 1113–1121, 2010.

[6] M. Putz, G. Schmidt, U. Semmler, M. Dix, M. Braunig, M. Brockmann, and S. Gierlings, "Heat flux in cutting: Importance, simulation and validation," *Procedia CIRP*, vol. 31, pp. 334–339, Apr. 2015. doi: 10.1016/j.procir.2015.04.088.

[7] J. Ji, Y. Huang, and K.-M. Lee, "A hybrid method based on macro–micro modeling and infrared imaging for tool temperature reconstruction in dry turning," *IEEE/ASME Trans. Mechatronics*, vol. 23, no. 3, pp. 1019–1027, Jun. 2018.

[8] A. H. Adibi-Sedeh, V. Madhavan, and B. Bahr, "Extension of Oxley's analysis of machining to use different material models," *J. Manuf. Sci. Eng.*, vol. 125, no. 4, pp. 656–666, 2003.

[9] M. U. Ghani, N. A. Abukhshim, and M. A. Sheikh, "An investigation of heat partition and tool wear in hard turning of H_{13} tool steel with CBN cutting tools," *Int. J. Adv. Manuf. Technol.*, vol. 39, nos. 9–10, pp. 874–888, 2008.

[10] H. Mzad, "A simple mathematical procedure to estimate heat flux in machining using measured surface temperature with infrared laser," *Case Stud. Therm. Eng.*, vol. 6, pp. 128–135, Sep. 2015.

[11] J. Taler, "Theory of transient experimental techniques for surface heat transfer," *Int. J. Heat Mass Transf.*, vol. 39, no. 17, pp. 3733–3748, 1996.

[12] F. Samadi, F. Kowsary, and A. Sarchami, "Estimation of heat flux imposed on the rake face of a cutting tool: A nonlinear, complex geometry inverse heat conduction case study," *Int. Commun. Heat Mass Transf.*, vol. 39, no. 2, pp. 298–303, 2012.

[13] C.-H. Huang and H.-C. Lo, "A three-dimensional inverse problem in predicting the heat fluxes distribution in the cutting tools," *Numer. Heat Transf. A, Appl.*, vol. 48, no. 10, pp. 1009–1034, 2005.

[14] R. Komanduri and Z. B. Hou, "Thermal modeling of the metal cutting process—Part II: Temperature rise distribution due to frictional heat source at the tool–chip interface," *Int. J. Mech. Sci.*, vol. 43, no. 1, pp. 57–88, 2001.

[15] C. Shan, X. Zhang, B. Shen, and D. Zhang, "An improved analytical model of cutting temperature in orthogonal cutting of Ti_6Al_4V," *Chin. J. Aeronaut.*, vol. 32, no. 3, pp. 759–769, 2019.

[16] Y. Huang and S. Y. Liang, "Cutting temperature modeling based on non-uniform heat intensity and partition ratio," *Mach. Sci. Technol.*, vol. 9, no. 3, pp. 301–323, 2005.

[17] J. Zhao and Z. Liu, "Effects of thermo-physical properties of $Ti_{0.41}Al_{0.59}N$ coating on transient and steady cutting temperature distributions in coated cemented carbide tools," *Int. Commun. Heat Mass Transf.*, vol. 96, pp. 80–89, Aug. 2018.

[18] J. Zhao, Z. Liu, B. Wang, Y. Hua, and Q. Wang, "Cutting temperature measurement using an improved two-color infrared thermometer in turning Inconel 718 with whisker-reinforced ceramic tools," *Ceram. Int.*, vol. 44, no. 15, pp. 19002–19007, 2018.

[19] W. Grzesik and P. Nieslony, "Physics based modelling of interface temperatures in machining with multilayer coated tools at moderate cutting speeds," *Int. J. Mach. Tools Manuf.*, vol. 44, no. 9, pp. 889–901, 2004.

[20] W. Grzesik and P. Nieslony, "A computational approach to evaluate temperature and heat partition in machining with multilayer coated tools," *Int. J. Mach. Tools Manuf.*, vol. 43, no. 13, pp. 1311–1317, 2003.

[21] J. Zhao, Z. Liu, Q. Wang, and J. Jiang, "Measurement of temperature-dependent thermal conductivity for PVD $Ti_{0.55}Al_{0.45}N$ ceramic coating by time domain thermo-reflectance method," *Ceram. Int.*, vol. 45, no. 7, pp. 8123–8129, 2019.

JINFU ZHAO received the B.S. degree in mechanical engineering from Shandong University, Ji'nan, China, in 2016, where he is currently pursuing the Ph.D. degree.

His research interests include material thermal properties and solid heat conduction of aerospace manufacturing process.

ZHANQIANG LIU received the B.S. and M.S. degrees in mechanical engineering from Shandong University, Ji'nan, China, in 1994, and the Ph.D. degree in philosophy from the City University of Hong Kong, Hong Kong, in 1999.

From 1999 to 2001, he was a Postdoctoral Fellow with the School of Mechanical Engineering, Shandong University. From 2001 to 2002, he was an Associate Professor with the School of Mechanical Engineering, Shandong University, where he has been a Professor, since 2002. His research interests include machining theory and tool technology. He is a member of the ASME and the Executive Director of the China Metal Cutting Tool Association.